nature photonics

LETTERS

PUBLISHED ONLINE: 21 NOVEMBER 2010 | DOI: 10.1038/NPHOTON.2010.255

An array of integrated atom–photon junctions

M. Kohnen, M. Succo, P. G. Petrov, R. A. Nyman*, M. Trupke† and E. A. Hinds*

Photonic chips that integrate optical elements on a single device can process vast amounts of information rapidly. A new branch of this technology involves coupling light to cold atoms or Bose–Einstein condensates, the quantum nature of which provides a basis for new information-processing methods. The use of optical waveguides gives the light a small cross-section, making coupling to atoms[1,2] efficient. In this Letter, we present the first waveguide chip designed to address a Bose–Einstein condensate along a row of independent junctions, which are separated by only 10 μm and have large atom–photon coupling. We describe a fully integrated, scalable design, and demonstrate 11 junctions working as intended, using a low-density cold atom cloud with as little as one atom on average in any one junction. The device suggests new possibilities for engineering quantum states of matter and light on a microscopic scale.

Microfabricated chips are widely used to control clouds of ultracold atoms and Bose–Einstein condensates (BECs)[3,4]. Recently, the idea has been extended to the control of ions[5], and there are similar possibilities for molecules[6]. This atom-chip technology provides a way to miniaturize existing atomic physics devices. In addition, it promises new devices that take advantage of the elementary quantum nature of atoms[7–9], ions[10] and molecules[6,11], together with photons[12]. Although laser light is an essential tool for preparing, controlling and interrogating the atomic systems on a chip, the integration of optics into atom chips is still in its infancy. Millimetre-sized vapour cells have enabled optical spectroscopy[13], clocks[14] and magnetometry on a chip, and etched mirrors on a silicon wafer have been used to integrate magneto-optical traps[15]. On a scale ten times smaller, several groups have explored how optical fibres, typically 125 μm in diameter, may be glued[16–18] or otherwise attached[19] to a chip. A pair of these fibres looking into each other can be used to detect an atom cloud and can reach close to single atom sensitivity[17]. When reflective coatings are added, the gap between two fibres[1,20], or between one fibre and a microfabricated mirror[21], becomes a Fabry–Pérot resonator. Similarly, a fibre can be coupled to a microdisk resonator[22,23]. These devices can achieve strong atom–photon coupling for applications in quantum information processing.

This Letter reports a further order of magnitude reduction in scale, in which the 125-μm-diameter optical fibre is replaced by integrated waveguides only 10 μm apart, with a 4-μm-square core. Because a BEC typically has a length of ∼100 μm, this reduction in size suggests the possibility of intersecting a BEC with many closely spaced atom–photon junctions of high coupling strength. In our device, illustrated in Fig. 1, a trench containing the cold atoms cuts through an array of 12 waveguides spaced by 10 μm. This design is a significant advance in the way that photons can be coupled to ultracold atoms.

To characterize the chip, we released cold atoms into a junction to measure its sensitivity and to demonstrate the basics of its operation. Every few seconds, ^{87}Rb atoms were cooled and collected from a room-temperature vapour by a low-velocity intense source (LVIS), then transferred to a magneto-optical trap (MOT) about 4 mm from the chip surface, where the atom density was up to 4×10^{-2} atoms per μm^3 and the temperature was ∼100 μK.

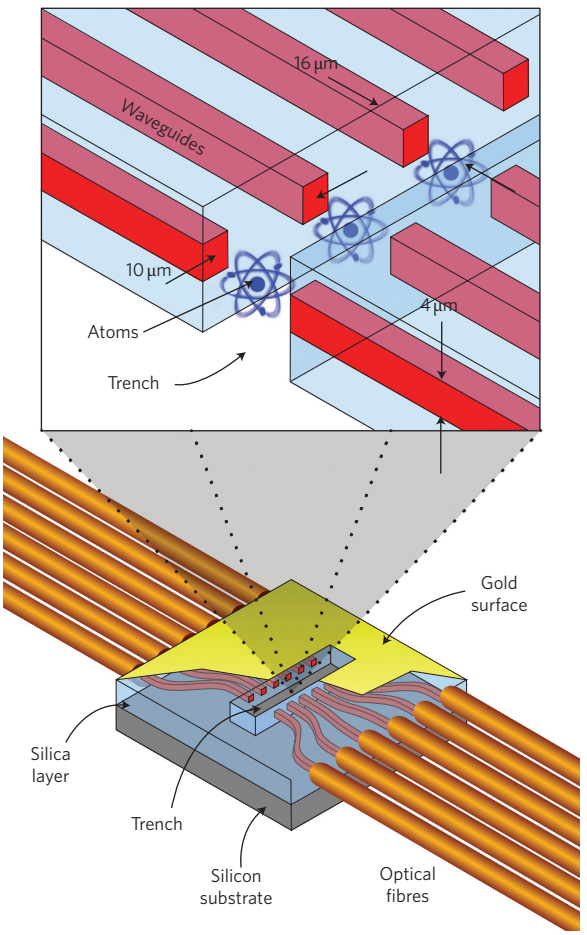

Figure 1 | Schematic of the integrated-waveguide atom chip. A silicon substrate supports a layer of silica cladding, within which 4-μm-square doped silica waveguide cores are embedded. There are 12 parallel waveguides (for clarity, only six are shown) spaced at the centre of the chip by 10 μm. These flare out at the edges of the chip so that optical fibres can be connected. A 22-μm-deep trench cutting across the waveguides is narrow enough (16 μm) that 65% of the light entering the trench is collected by the waveguides on the far side in the absence of atoms. An atom in the trench affects the phase and the intensity of the transmitted light. Conversely, the light affects the state of the atom. Thus, each waveguide comprises a microscopic atom–photon junction. The top layer of the chip is coated with gold to reflect the laser light used for cooling the atoms. Current-carrying wires below the chip provide magnetic fields to trap and move the atoms.

Centre for Cold Matter, Blackett Laboratory, Imperial College London, Prince Consort Road, London SW7 2BW, UK; †Present address: Atominstitut der Österreichischen Universitäten, Stadionallee 2, 1020 Wien, Austria. *e-mail: r.nyman@imperial.ac.uk; ed.hinds@imperial.ac.uk

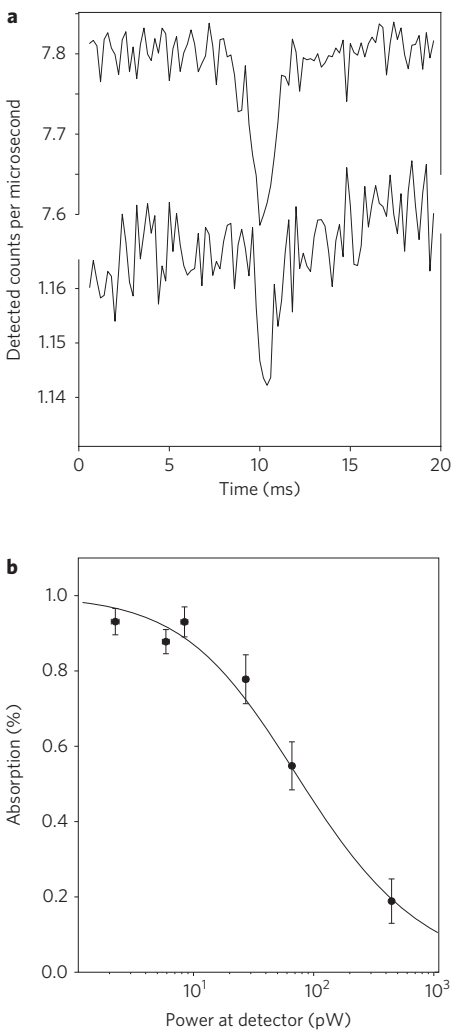

Figure 2 | Absorption of light by atoms in the trench. a, Time-of-flight signals from two adjacent junctions. Upper curve: the photodiode detects 7.8×10^6 counts per second (5 pW). The 2.6% dip indicates 8×10^{-3} atoms per μm^3, that is, one atom, on average, in the illuminated volume, ~100 μm^3. Lower curve: the adjacent channel shows the same atom density and transit time, because the 10-μm channel spacing is much less than the cloud size. A smaller photon rate gives a lower signal-to-noise ratio. **b**, Measured fraction of light absorbed by atoms versus detected power. The solid line (theory) takes into account variations of light intensity and optical pumping of atoms (see Methods, 'Saturation intensity I_{sat}'). There are two fitting parameters: atom number density, and the ratio of light power in the trench to that at the avalanche photodiode (setting the power axis scale). The fit tells us that the power in the trench is six times that at the detector, consistent with the known transmission of 65% across the trench and 25% through the fibre couplers on the way to the detector. Error bars indicate 1σ statistical uncertainties for Poissonian light with detector dead time.

This cloud was pushed towards the chip just before switching off the MOT light and magnetic field, thereby launching the atoms at 40 cm s^{-1} into the trench. The light beams from the waveguides diverged only slightly as they crossed the trench, with w (the $1/e$ radius of the field) growing from 2.2 μm to 2.8 μm. As the width of the trench was $L = 16$ μm, any given beam interacted with approximately one to four atoms of the cloud as they passed through. Each atom crossed the light in ~7 μs, scattering up to 130 photons (fully saturated rate, $\Gamma/2 = 1.9 \times 10^7\ s^{-1}$).

With low-intensity resonant light in the trench at a frequency $\omega = 2\pi \times 385$ THz, and rubidium atoms of number density ρ, we expect the absorbed fraction of the light f to be given by

$$f = \frac{\hbar\,\omega\Gamma L}{2I_{sat}}\rho = 3.2\ \mu m^3 \times \rho \qquad (1)$$

The saturation intensity I_{sat} depends on the polarization of the atoms and the light, and for our first experiments it is well approximated by $I_{sat} = 22$ pW μm^{-2} (see Methods, 'Saturation intensity I_{sat}'). The atoms in our experiment should therefore absorb up to 12% of the light. This is demonstrated experimentally in Fig. 2a, where two adjacent channels of the chip record the density of atoms versus time at positions 10 μm apart. As the cloud is much larger than the channel spacing, the absorption dips recorded by the two junctions are the same. They occur about 10 ms after the atoms are launched into the trench and have the expected size and width.

If the intensity in the trench I approaches I_{sat}, the scattering rate begins to saturate and the absorbed fraction decreases according to the relation

$$f(I) = \frac{f(I \to 0)}{1 + I/I_{sat}} \qquad (2)$$

The bleaching of the atoms in this way allows the absolute intensity of the light in the trench to be measured. Figure 2b shows the measured decrease of absorption as the detected power is increased, together with a fitted theoretical curve. The fit relates intensity in the trench to power at the detector, and demonstrates that the latter is six times smaller than the power in the trench, as expected (see Methods, 'Detection system'). These experiments show that the junction works: the light detects the atoms, the atoms sense the light, and both perform in agreement with theory.

For some applications it will be important to control the polarization of the light in the trench as well as its intensity. We find

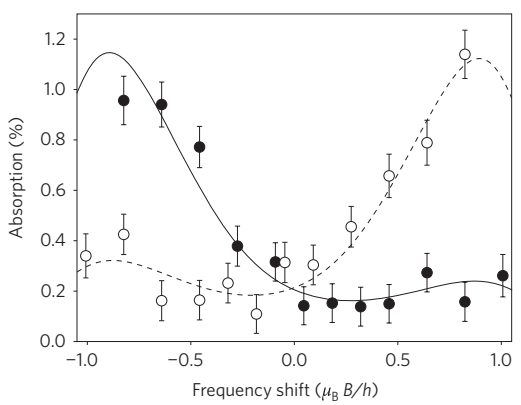

Figure 3 | Zeeman-split absorption spectrum measures light polarization. D_2 absorption spectrum of ^{87}Rb, measured on the hyperfine component $|F = 2\rangle \to |F' = 3\rangle$ with a magnetic field of 0.78 mT parallel to the waveguides. When pure ξ^- light (filled circles) is coupled into the input fibre, the Zeeman shift is almost $-\mu_B B/h$. The line is a theory obtained by summing over all the Zeeman components of the spectrum, fitted to the data with two parameters: the overall normalization and the ratio of ξ^+ and ξ^- intensity. This fit tells us that (85±3)% of the power in the trench is still in the ξ^- mode. For ξ^+ light (open circles) the shifts are opposite. The fit to these points gives (81±3)% of power in the ξ^+ mode. The experiment was carried out at sufficiently low light intensity that optical pumping was negligible, allowing the theory to take equal populations of the m_F levels. Error bars indicate 1σ statistical uncertainties for Poissonian light with detector dead time.

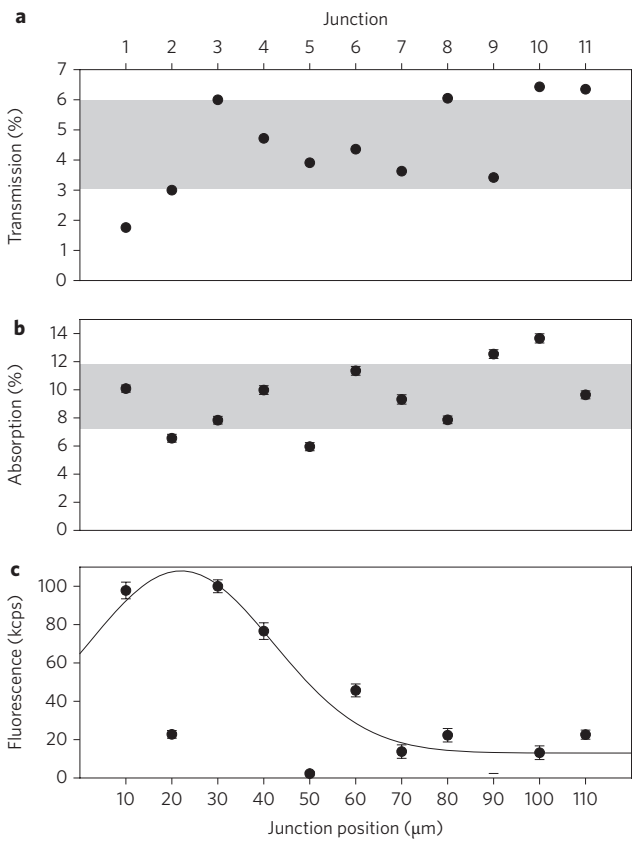

Figure 4 | Comparison of performance for 11 junctions. a, Optical transmission efficiency of the waveguides. Grey bar: mean and standard deviation. **b**, Absorption due to atoms, for densities around 4×10^{-2} atoms per μm^3. Error bars indicate the statistical noise of the light. Some additional variation is due to fluctuations in atom density. Grey bar: mean and standard deviation. These 11 junctions are working well. **c**, Fluorescence. Points show peak detected count rates due to atomic fluorescence, excited by an external, resonant beam focused to a $1/e$ field radius of 40 μm. The line is a Gaussian profile with a width corresponding to the known beam size, with an added background offset. The junctions act as pixels, spaced by 10 μm, allowing the profile of the excited atom cloud to be measured. Error bars indicate the statistical noise of the light. Some additional variation is due to fluctuations in atom density. Junctions 2, 5 and 9 appear to be partially defective, although they work well in transmission and absorption.

that light prepared with positive helicity, ξ^+, and delivered to the chip through one of the optical fibres, still has typically 87% of the power in the ξ^+ mode when it emerges from the corresponding output fibre, provided the fibres are securely held so that they cannot move in the ambient currents of air. (The fibres were not well fixed for the experiments of Fig. 2, where the polarization was random.) This suggests that the light in the trench is polarized, but we were also able to check the polarization directly, using the atoms themselves as the probe.

Figure 3 shows the absorption of light versus frequency in the presence of a magnetic field, $B = 0.78$ mT, parallel to the waveguides. This spectrum indicates the ratio of σ^+ to σ^- power in the trench, where $\sigma^+(\sigma^-)$ indicates that the angular momentum of the light is parallel (antiparallel) to the magnetic field. The light excites the ^{87}Rb D_2 transition $|F=2,\ m_F\rangle \rightarrow |F'=3,\ m'_F\rangle$, for which the Zeeman shift of $\sigma^\pm$ transitions is $(1/6)(m_F \pm 4)\mu_B B/h$, where m_F is the projection of atomic angular momentum, and $\mu_B/h = 14$ GHz T^{-1}. The strongest excitation with $\sigma^+(\sigma^-)$ light comes from $m_F = +2(-2)$ and is shifted by $+(-)\mu_B B/h$. With ξ^- input light (filled circles) the strong peak is close to $-\mu_B B/h$, indicating that the power in the trench is still mainly of ξ^- polarization. When we reverse the helicity (open circles) the shift reverses. We conclude that the polarization in the trench can be controlled by adjusting the input light to have up to 90% of the power in pure ξ^+ or ξ^- polarization.

Figure 4 shows a comparison of the performance of 11 junctions. Net transmission of light through the chip and fibres was in the range 2–6% (Fig. 4a). The atom absorption signals were compared using a large cloud to give equal density in all the junctions (Fig. 4b). The variability is small and mainly due to fluctuations in atom density between separate channel tests. To demonstrate high spatial resolution, a small part of the cloud was excited with resonant light focused to a 40-μm spot at one end of the trench. Figure 4c shows fluorescence signals that closely follow the excitation beam profile. A low level of background fluorescence is seen in all channels. This may be due to defects that scatter light into the trench and then to the detector via the atoms. The poor performance in fluorescence detection of junctions 2, 5 and 9 may be related to the same phenomenon.

In conclusion, we have fabricated and demonstrated an array of 12 atom–photon junctions, fully integrated on a chip using a scalable design. This device is a major advance over previous interfaces between light and BEC because it provides a way to probe or alter the structure of a BEC at points only 10 μm apart. To demonstrate this, we have shown that a low density of atoms can be detected, corresponding to less than one atom in the light mode. We have shown, using the atoms themselves, that the polarization and intensity of the light in the trench can be reliably controlled. The scalability has been tested by connecting a full set of 24 fibres to one of the chips and demonstrating sensitive absorption detection in 11 junctions. High spatial resolution is demonstrated by measuring the profile of a small optically excited atom cloud by observation of its fluorescence. Our next step will be to bring a trapped BEC into the trench. These clouds have a typical density of 100 atoms per μm^3 and will therefore be opaque at resonance. If off-resonant measurements[24] are used, much less than one photon per atom can be scattered, while retaining sufficient sensitivity to make precise measurements of local density in a single shot as short as 1 μs. These atom–photon junctions suggest new possibilities for engineering the quantum states of matter and light on a microscopic scale.

Methods

Photonic chip fabrication. The chip was manufactured by the Centre for Integrated Photonics (Ipswich, UK) on a 1-mm-thick silicon wafer. A 10-μm-thick layer of silica, grown by thermal oxidation, formed the lower cladding for the waveguides. A second layer of silica, doped with germanium and boron to achieve a 0.75% refractive-index contrast, was created by flame hydrolysis deposition. This was etched through a UV-lithography mask to create the waveguide cores. A further 10-μm silica layer of upper cladding, also deposited by flame hydrolysis, was doped with boron and phosphorus to match the refractive index of the lower cladding. A layer of 50 nm of chrome and then 100 nm of gold provided the reflecting surface needed by the MOT beams. Finally the central trench was cut by deep reactive ion etching to a depth of 22 μm through a 16 μm × 500 μm rectangular mask formed by UV-lithography. The finished chip was polished on the back to reduce its thickness to 500 μm. This reduced the distance between the atoms in the trench and the current-carrying wires underneath.

The chip was glued to a sub-chip containing current-carrying wires. These provide magnetic fields for preparing the BEC and generate the field parallel to the waveguides that is used in the experiments of Fig. 3. The two adjacent channels used in making Figs 2 and 3 were connected by glueing four single-mode fibres (non-polarization-maintaining) to the polished edges of the chip using Epotek 353ND index-matching adhesive. The entire optical path from fibre input to fibre output had 5% transmission. This comprised 50% from each of the two vacuum feedthroughs, 60% from each fibre/waveguide interface, 78% at each face of the trench (Fresnel reflection plus roughness) and 83% mode overlap where the expanded beam arrives at the second waveguide. The various interfaces in the optical train form several etalons that modulate the transmission by a few percent as the frequency varies. The crosstalk between the waveguides was less than 10^{-3}.

The data in Fig. 4 come from a second chip, with a full set of junctions connected using a commercial strip of 12 fibres attached to V-grooves in a carrier, spaced to match the waveguide positions on the chip. The first and last fibres were positioned

so that their couplings were optimized and the whole assembly was held in place using Epotek OG116. This index-matching glue is a better choice than 353ND because it is both UV-curing and bakeable, as required for ultrahigh vacuum. We have connected several chips in this way, and normally find transmissions in the range 20–30%, which vary because the fibre cores are not all perfectly centred on the waveguides. The net transmission would ideally be 30%, comprising 80% from mode overlap at each fibre and 50% across the trench. The fibre coupling could approach 100% if the fibre mode size was matched to the 2.16 μm waveguide mode instead of using standard fibres with a mode of 3.6 μm. The trench transmission could reach 74% if the machining were improved to eliminate the roughness of the waveguide ends. Unusually, the particular chip used to make Fig. 4 lost one channel during glueing of the fibres. In addition, this chip was mounted on a sub-chip, which, due to a design flaw, interfered with one of the fibre carriers and reduced the transmission by about a factor of four below the normal level. For the data presented here, the photodetector was coupled to the correctly connected side of the chip. We also changed the vacuum feedthroughs to those described by Abraham and Cornell[25], which have 100% transmission.

Detection system. The light was transported by optical fibres to a single-photon counting avalanche photodiode (APD). The counting rates in these experiments were between 7×10^4 and 1.5×10^7 counts per second (cps), far above the background of ~130 cps from dark counts and stray light. At the high end, almost half the counts were lost to the 32-ns dead time of the detector, which limits the rate. We extended the dynamic range by using calibrated filters to attenuate the light. We checked and confirmed the manufacturer's specified dead time by measuring the noise as a function of intensity and comparing this with the Poisson statistics appropriate for attenuated laser light.

Our measurements of absorption were taken over a number of shots, ranging from 10 to 600. The APD signal was averaged, then smoothed over a 1–2-ms window as appropriate, before taking the reading at the point in time where the atom density in the trench was at its maximum. For the polarization measurements the large magnetic field needed time to settle after switching on, so the measurement point was delayed. Each of these measurements was accompanied by a background measurement without atoms, which was averaged and used to normalize the absorption. The error bars indicate the 1σ statistical uncertainties of a Poissonian photon source with detector dead time[26].

Saturation intensity I_{sat}. Light is at the saturation intensity I_{sat} when the photon scattering rate from one atom is $\Gamma/4$. Here, Γ is the population decay rate of the upper state and is the same regardless of which magnetic sub-level is excited. Among the D_2 transitions $|F=2,m_F\rangle \rightarrow |F'=3, m_F'\rangle$ of ^{87}Rb, the strongest are $m_F=\pm 2 \rightarrow m_F'=\pm 3$ driven by $\xi^{\pm}$ light. Both of these have I_{sat}= 16.7 pW μm^{-2}. The relative strengths of the other transitions depend only on the squares of the $3-j$ symbols

$$\begin{pmatrix} 3 & 1 & 2 \\ -m_F' & -m_F'+m_F & m_F \end{pmatrix}^2$$

A magnetic field is applied along the waveguides, so the light only has $\xi^{\pm}$ polarizations and the transitions are restricted to $m_F'=m_F\pm 1$.

For the experiments in Fig. 2, the atoms scatter several photons, even in the most weakly excited sub-level, and this ensures that the cloud is optically pumped. To a good approximation, the resulting population distribution of m_F states is the steady state of the Einstein rate equations. We calculate the mean scattering rate using that distribution. The calculation is repeated to average over all polarizations of the light because our measurements are an average over many shots, each with random polarization. Thus, we obtain an effective saturation intensity of I_{sat} = 22.4 pW μm^{-2}.

Received 24 December 2009; accepted 29 September 2010; published online 21 November 2010

References

1. Horak, P. *et al.* Possibility of single-atom detection on a chip. *Phys. Rev. A* **67,** 043806 (2003).
2. Bajcsy M. *et al.* Efficient all-optical switching using slow light within a hollow fiber. *Phys. Rev. Lett.* **102,** 203902 (2009).
3. Fortágh, J. & Zimmermann, C. Magnetic microtraps for ultracold atoms. *Rev. Mod. Phys.* **79,** 235–289 (2007).
4. Reichel, J. & Vuletic, V. *Atom Chips* (Wiley-VCH, in the press).
5. Seidelin, S. *et al.* Microfabricated surface-electrode ion trap for scalable quantum information processing. *Phys. Rev. Lett.* **96,** 253003 (2006).
6. André, A. *et al.* A coherent all-electrical interface between polar molecules and mesoscopic superconducting resonators. *Nature Phys.* **2,** 636–642 (2006).
7. Jaksch, D., Briegel, H.-J., Cirac, J. I., Gardiner, C. W. & Zoller, P. Entanglement of atoms via cold controlled collisions. *Phys. Rev. Lett.* **82,** 1975–1978 (1999).
8. Chen, S. *et al.* Deterministic and storable single-photon source based on a quantum memory. *Phys. Rev. Lett.* **97,** 173004 (2006).
9. Gleyzes, S. *et al.* Towards a monolithic optical cavity for atom detection and manipulation *Eur. Phys. J. D* **53,** 107–111 (2009).
10. Cirac, J. I. & Zoller, P. Quantum computations with cold trapped ions. *Phys. Rev. Lett.* **74,** 4091–4094 (1995).
11. DeMille, D. Quantum computation with trapped polar molecules. *Phys. Rev. Lett.* **88,** 067901 (2002).
12. Politi, A., Cryan, M. J., Rarity, J. G., Yu, S. & O'Brien, J. L. Silica-on-silicon waveguide quantum circuits. *Science* **320,** 646–649 (2008).
13. Yang, W. *et al.* Atomic spectroscopy on a chip. *Nature Photon.* **1,** 331–335 (2007).
14. Knappe, S. *et al.* A microfabricated atomic clock. *Appl. Phys. Lett.* **85,** 1460–1462 (2004).
15. Pollock, S., Cotter, J. P., Laliotis, A. & Hinds, E. A. Integrated magneto-optical traps on a chip using silicon pyramid structures. *Opt. Express* **17,** 14109–14114 (2009).
16. Quinto-Su, P., Tscherneck, M., Holmes, M. & Bigelow, N. On-chip optical detection of laser cooled atoms. *Opt. Express* **12,** 5098–5103 (2004).
17. Eriksson, S. *et al.* Integrated optical components on atom chips. *Eur. Phys. J. D* **35,** 135–139 (2005).
18. Takamizawa, A., Steinmetz, T., Delhuille, R., Hänsch, T. W. & Reichel, J. Miniature fluorescence detector for single atom observation on a microchip. *Opt. Express* **14,** 10976–10983 (2006).
19. Wilzbach, M. *et al.* Simple integrated single-atom detector. *Opt. Lett.* **34,** 259–261 (2009).
20. Colombe, Y. *et al.* Strong atom–field coupling for Bose–Einstein condensates in an optical cavity on a chip. *Nature* **450,** 272–276 (2007).
21. Trupke, M. *et al.* Atom detection and photon production in a scalable, open, optical micro-cavity. *Phys. Rev. Lett.* **99,** 063601 (2007).
22. Dayan, B. *et al.* A photon turnstile dynamically regulated by one atom. *Science* **319,** 1062–1065 (2008).
23. Aoki, T. *et al.* Efficient routing of single photons by one atom and a microtoroidal cavity. *Phys. Rev. Lett.* **102,** 083601 (2009).
24. Hope, J. J. & Close, J. D. General limit to nondestructive optical detection of atoms. *Phys. Rev. A* **71,** 043822 (2005).
25. Abraham, E. R. I. & Cornell, E. A. Teflon feedthrough for coupling optical fibers into ultrahigh vacuum systems. *Appl. Opt.* **37,** 1762–1763 (1998).
26. Yu, D. F. & Fessler, J. A. Mean and variance of single photon counting with deadtime. *Phys. Med. Biol.* **45,** 2043–2056 (2000).

Acknowledgements

The authors acknowledge valuable discussions with B. Darquié, the assistance of G. Lepert with fibre coupling, and the technical expertise of J. Dyne, S. Maine and V. Gerulis, without whom the apparatus could not have been constructed. We acknowledge UK support by the Engineering and Physical Sciences Research Council (EPSRC), the Quantum Information Processing Interdisciplinary Research Collaboration (QIPIRC) and the Royal Society, and European Union support through Scalable Quantum Computing with Light and Atoms (SCALA) and Hybrid Information Processing (HIP).

Author contributions

R.A.N., M.S., M.K. and P.G.P. constructed the apparatus, maintained the experiment, and took and analysed the data. M.T. and M.K. designed, specified and assembled the waveguide chip. E.A.H. was the principal investigator and also co-wrote the manuscript with R.A.N. All authors commented on the manuscript and discussed the construction, data, its analysis and interpretation.

Additional information

The authors declare no competing financial interests. Reprints and permission information is available online at http://npg.nature.com/reprintsandpermissions/. Correspondence and requests for materials should be addressed to R.A.N. and E.A.H.